REVISION 3

Dissolved silica-catalyzed disordered dolomite precipitation

Yihang Fang[1], and Huifang Xu[1*]

[1] NASA Astrobiology Institute, Department of Geoscience, University of Wisconsin–Madison, 1215 W Dayton St, Madison, Wisconsin, 53706, USA

*Corresponding author: hfxu@geology.wisc.edu

ABSTRACT

There is a great abundance of sedimentary dolomite in the Proterozoic and Lower Paleozoic, but examples of primary dolomite are scarce in the Cenozoic. This discrepancy suggests a poorly understood, but dramatic shift in the geochemical system that inhibited dolomite formation. Previous research on microbial-mediated dolomite formation demonstrated that microbial activity can promote disordered dolomite precipitation through the catalytic role of polysaccharides. However, the microbial-mediated model cannot explain some of the Precambrian dolomite for which there is no evidence of microbial origin. Here, we present an abiotic mechanism with dissolved silica catalyzed dolomite precipitation that provides new insight into this long-lasting "dolomite problem". In this study, we demonstrate that the presence of 1-2 mM of aqueous $Si(OH)_4$ in high Mg:Ca ratio solutions at room temperature will promote disordered dolomite precipitation (with up to 48.7 mol.% $MgCO_3$) and inhibit aragonite formation. Dissolved silica in solution also promotes Mg incorporation into the Ca-Mg carbonates. Dissolved silica possesses low dipole moment and dielectric constant similar to hydrogen sulfide, dioxane, polysaccharide and exopolymeric substances (EPS), which are catalysts in previous established room temperature dolomite synthesis. The molecules with low dipole moment adsorbed on the dolomite surface can lower the dehydration energy barrier of a surface Mg^{2+}-water complex and promote dolomite nucleation and growth. This study provides a new model for abiotic sedimentary dolomite formation which is likely to be responsible for the significant amount of primary dolomite in the Earth history.

Keywords: Disordered dolomite, dolomite problem, sedimentary dolomite, dissolved silica

INTRODUCTION

In spite of extensive research, dilemmas and puzzles surrounding the formation mechanism of dolomite linger on. Although dolomite is the thermodynamically favored product in seawater and many other natural saline/hypersaline bodies of water, dolomite is rarely found in the modern environment. The difficulty in understanding sedimentary dolomite formation comes from the scarcity of modern examples and the inability to precipitate dolomite from seawater at surface temperature. Although modern seawater is supersaturated with respect to dolomite, primary dolomite has mostly been reported in limited settings such as alkaline lakes (Peterson et al. 1963; Rosen et al. 1988; Last 1990), deep marine carbonate pavements associated with methane seeps (Lumsden 1988; Gregg and Frank 2009; Xu 2010; Lu et al. 2018) and shallow marine environments with microbial mats (Curtis et al. 1963; Kendall and Skipwith 1968; Vasconcelos and McKenzie 1997; Meister et al. 2007; Zhang et al. 2015). Land (1998) concluded after a 32-year experiment with a 1000-fold oversaturated solution at room temperature which failed to precipitate dolomite that the "dolomite problem" results from the kinetic inhibition of dolomite crystallization. One of the main issues is that the Mg^{2+} cation possesses a high affinity for water and forms a hydration layer that inhibits dolomite growth (Lippmann 1973; Berner 1975). Therefore, dolomite formation at low temperature requires the presence of a catalyst to destabilize the surface Mg^{2+}-water complex (Shen et al. 2015).

Most of the Ca-Mg carbonate that approaches the stoichiometric composition of dolomite found in recent sediments displays little to no ordering (Land 1980; Fang and Xu 2019). Cation ordering in dolomite refers to alternating calcium and magnesium layers along the ***c*** axis that results in a reduced $R\bar{3}$ symmetry relative to the $R\bar{3}c$ symmetry of calcite. Although

thermodynamics favors the ordered dolomite structure, the ordering process is kinetically inhibited at low temperatures. Partially ordered "protodolomite", a term proposed by Graf and Goldsmith (1956), with weak or absent ordering is believed to be the precursor to sedimentary dolomite (Zhang et al. 2012b; Gregg et al. 2015; Kaczmarek et al. 2017). Gregg et al. (2015) refer to Ca-Mg carbonates without ordering as "very high-magnesium calcite (VHMC)" and Sibley et al. (1994) suggest VHMC has a composition of 35-40 mol.% $MgCO_3$. In this study, we use the term "disordered dolomite" to refer to Ca-Mg carbonates containing over 36 mol.% $MgCO_3$ with no cation ordering, whereas materials described as "protodolomite" display weak to moderate ordering. The composition range of "disordered dolomite" is determined by the extent of cation ordering observed in natural samples (Fang and Xu 2019).

Previously published disordered dolomite synthesis experiments usually require the presence of low dipole moment catalysts such as hydrogen sulfide (Zhang et al. 2012a, 2013), dioxane (Oomori and Kitano 1987), polysaccharides and exopolymeric substances (EPS) (Zhang et al. 2012b, 2015). Previous studies have recognized a positive relationship between microbial activity and sedimentary dolomite (Kendall and Skipwith 1968; Hardie 1987; Vasconcelos and McKenzie 1997; Warren 2000; Zhang et al. 2015). Substances such as polysaccharides and EPS from a microbial mat and dissolved sulfide from microbial respiration are shown to successfully catalyze Mg^{2+} dehydration and dolomite formation in ambient conditions (Zhang et al. 2012a, 2012b, 2015, 2021; Shen et al. 2014, 2015). However, the microbial-mediated dolomite formation model is unable to explain all dolomite deposits in the Archean, Proterozoic and early-Paleozoic when microbial activity is thought to have been relatively low compared to the high level of microbial productivity observed in the present day, which generates a comparatively insignificant amount of dolomite in modern sediments (Awramik and Sprinkle 1990). Macrostrat,

a platform that compiles spatial and temporal geological data, shows that some primary dolomite in the Proterozoic is not correlated with stromatolite occurrences, indicating that an abiotic mechanism can drive dolomite precipitation (Supplemental figure 1; Peters et al., 2017). Further, these factors suggest that an abiotic mechanism may have been involved in the formation of sedimentary dolomite deposited early in Earth's history. Some modern playa lakes and restricted lagoons with dolomite and protodolomite precipitation contain elevated dissolved silica ranging from ~1.0 mM to 1.8 mM in addition to the microbial activities that occur in the ambient environment (Jones et al., 1967; Stoessell and Hay, 1978; Muir et al., 1980; Last, 1990). This study investigates the influences of dissolved silica on the formation of Ca-Mg carbonates and presents a dolomite precipitation model whereby dissolved silica catalyzes the reaction abiotically, complementing the existing microbial-mediated mechanism.

METHODS

Synthesis experiment

Experiments were performed with 30 mM or 50 mM $MgCl_2 \cdot 6H_2O$, 10 mM $CaCl_2 \cdot 2H_2O$, 50 mM NH_4CO_3, and 1-2 mM $Na_2SiO_3 \cdot 9H_2O$. The Mg to Ca ratio of the solutions were set at 5:1 and 3:1 to simulate modern and ancient seawater Mg:Ca ratios. After stirring for 30 minutes, solutions were divided into 100 mL sealed bottles and kept at 20°C and 40°C. All experimental vessels were washed consecutively with 1 mM HCl, DI water, ethanol, and DI water, and dried in an oven at 110°C for 1 day to avoid carbonate and biomass contamination. Solutions were filtered after 4 weeks and precipitates were rinsed with DI water then air-dried.

Powder X-ray diffraction

Powder X-ray diffraction (XRD) was performed using a Rigaku Rapid II X-ray diffraction system with Mo Kα radiation. This XRD instrument uses a 2-D image-plate detector for signal collection and integrates using Rigaku's 2DP software. XRD was run at 50 kV and with a 100-μm diameter collimator. Powder samples were packed into 1.1 mm diameter polyimide tubes with a 0.5 mm wall thickness. Mineral identification was performed using the MDI Jade 9.5 software package with the American Mineralogist Crystal Database (AMCSD) and the PDF-4+ database from the International Centre for Diffraction Data (ICDD). Rietveld refinements for phase percentage and unit-cell parameters were run using Bruker's TOPAS software and crystal structures from the AMCSD. Pearson VII peak functions were used for all refinements.

Scanning electron microscopy, transmission microscopy and X-ray energy dispersive spectroscopy

Scanning electron microscopy (SEM) analyses were carried out using a Hitachi S3400 at 15 kV. Energy-dispersive X-ray spectroscopy (EDS) analyses were carried out using an AZtecOne system with silicon drift detector from Oxford Instruments. Transmission electron microscopy (TEM) experiments were conducted using a Tecnai T12 with a 120 kV acceleration voltage. The average $MgCO_3$ mol.% of disordered dolomite and Mg-calcite were calculated on the basis of the d_{104} value using a disordered contouring line (Zhang et al. 2010; Fang and Xu 2019). Compositions of the precipitated Ca-Mg carbonates were also confirmed with X-ray EDS from SEM and TEM. Dolomite standard from Delight, Baltimore with 50.48 mol.% $MgCO_3$ (Zhang et al., 2012; Fang and Xu, 2019) was used to calibrate the k-factor for the intensity ratio method for the TEM-based X-ray EDS (Cliff and Lorimer, 1972; Cliff and Lorimer, 1975). This method has an estimated error within 2 mol. %. Scanning-transmission electron microscopic imaging was

carried out using a FEI Talos F200X system with high-angle annular dark field (HAADF) imaging mode and X-ray energy-dispersive spectroscopy (XEDS) spectroscopic imaging.

Adsorption experiments

Adsorption experiments were performed using a colorimetric heteropoly blue method (Clesceri et al. 1999). This method was used to measure molybdate-reactive silicon including monomeric silica and some low-weight silica oligomers. Ground calcite and dolomite chalk were added into a solution containing 0.5- 1.4 mM of dissolved silica at pH~8.5. The solid to solution ratio was set to 1g/L following Zhang et al. (2012a). The calcite and dolomite powders had surface areas of ~9.8 m^2/g and 6.6 m^2/g, respectively (as determined by the multipoint N_2-BET method). Solutions were prepared with 50 mM $NaHCO_3$, 120 mM NaCl, and 0.5 - 1.4 mM $Na_2SiO_3 \cdot 9H_2O$ and did not contain calcium or magnesium to avoid Ca-Mg carbonate precipitation. Solutions were ultrasonicated to suspend the ground chalk then put into shaker for 24 hours for the carbonate to adsorb silica. Ammonium molybdate was added into the Si-bearing solutions which were then reduced by the addition of 1-amino-2-naphthol-4-sulfonic acid to produce blue Si complexes. The light absorbance of samples was measured using a spectrophotometer at 815 nm. A standard calibration curve relating silica concentration to light absorbance was constructed at the beginning of each analytical session. The precision of the colorimetric method is ~5% (Clesceri et al. 1999).

RESULTS

Solution pH change

During the synthesis experiments with dissolved silica, precipitation of carbonates was observed after 1-2 hours as indicated by the appearance of cloudiness in the previously clear solutions. In the control solution without dissolved silica, precipitation also occurred shortly after mixing of $MgCl_2 \cdot 6H_2O$, $CaCl_2 \cdot 2H_2O$, and NH_4CO_2. Solution pH decreased slightly from 8.46 - 9.17 to 8.27 - 8.87 (Table 1) due to carbonate precipitation.

X-ray diffraction

Powder XRD analyses show that most of the precipitated Ca-Mg carbonates are in the dolomite composition range. Mole percentages of $MgCO_3$ were estimated from the empirical correlation d_{104} on the disorder contour line (Zhang et al., 2010; Fang and Xu, 2019). Ca-Mg carbonates with an average composition of ~48.7 mol. % $MgCO_3$ and aragonite were precipitated in solution with an initial Mg:Ca ratio of 5:1 and 2 mM of dissolved silica at 20°C (Figure 1C and Table 1). The solutions with a 5:1 Mg:Ca ratio and 1 mM of dissolved silica at 20°C show Ca-Mg carbonate at a lower average mol.% $MgCO_3$ of ~41.9%. Solutions with a Mg:Ca ratio of 3:1 produced Ca-Mg carbonates with ~32.3 – 37.1 mol.% $MgCO_3$ and some aragonite for all temperature conditions with dissolved silica (Figure 1 & 2 and Table 1). The unit cell parameters of the Ca-Mg carbonates derived from Rietveld refinement also show a decrease in both the *a*- and *c*-axis lengths, decreasing from 4.889(3) Å and 16.577(12) Å to 4.853(3) Å and 16.434(21) Å, respectively; this corresponds to a compositional range of 32.3 mol.% $MgCO_3$ to 48.7 mol.% $MgCO_3$ consistent with the observed variation in d_{104} values. XRD patterns did not demonstrate any "*b*"-reflection or ordering peaks for the precipitated Ca-Mg carbonate in the dolomite range indicating that the precipitated carbonates are disordered dolomite. On the other hand, aragonite and small amounts of Mg-bearing calcite with ~8.1 mol.% $MgCO_3$ were precipitated from the control solution with an initial Mg:Ca ratio of 5:1 without dissolved silica at 20°C (Figure 1C

and Table 1). When solutions were placed in the oven at 40°C for 4 weeks, a mixture of carbonates including Ca-Mg carbonates with ~ 43.9 - 44.9 mol.% $MgCO_3$, small amounts of aragonite and hydromagnesite (a metastable hydrous Mg-carbonate phase $Mg_5(CO_3)_4(OH)_2 \cdot 4H_2O$) were precipitated in solutions with 1 and 2 mM of dissolved silica (Figure 1A and Table 1). XRD patterns of samples with high amorphous background also did not detect any Mg-silicate such as sepiolite, saponite, kerolite or palygorskite indicating possible amorphous Mg-silicate precipitation (Figure 1A).

SEM

SEM-based X-ray energy-dispersive spectroscopy (EDS) analyses confirm the compositions of Ca-Mg carbonate crystallized in dissolved silica bearing solution are in the dolomite composition range with 43 – 47 mol.% $MgCO_3$ (Figure 3). With a Mg:Ca ratio of 3:1, increasing dissolved silica from 1 mM to 2 mM results in a mol.% $MgCO_3$ increase from 32.4% to 43.1%, which is mostly consistent but slightly higher at elevated silica concentrations compared to the XRD results. Similarly, with a Mg:Ca ratio of 5:1, increasing silica from 1 mM to 2 mM results in an increase in mol.% $MgCO_3$ from 44.9% to 47.1%, which is also within the estimated range of the XRD data. SEM images of synthetic carbonates show that Ca-Mg carbonates of dolomitic composition forms spherulites (Figure 3); these are commonly found as dumbbell shaped masses ~5 μm in diameter, which is similar to the morphologies of strontium and barium carbonates observed by García-Ruiz (1998). Some spherulites seem to be hollow at the center (Figure 3C). At 40°C, spherulites (~2 μm diameter) usually form platy aggregates (Figure 3B). Close-up observation shows that these Ca-Mg carbonates form as nanocrystals with sizes smaller than 100 nm (Figure 3). SEM imaging also identifies fibrous and equant Mg-silicate phases (Figure 3C).

No significant morphology changes in the disordered dolomite were observed between different dissolved silica concentrations and Mg:Ca ratios.

TEM and STEM

TEM- X-ray EDS analyses also confirm the compositions of Ca-Mg carbonate as 44 – 54 mol.% $MgCO_3$ (Figure 4A). Selected area electron diffraction (SAED) patterns on the [010] zone-axis shows that none of the carbonate crystals display "*b*"-reflections which would indicate Ca-Mg ordering in the dolomite structure. Therefore, these synthetic Ca-Mg carbonates with dolomite composition are completely disordered and we refer to them as disordered dolomite (Fang and Xu 2019). TEM images show these nano-crystals are smaller than 100 nm in size. Individual disordered dolomite nano-crystals have distinct (104) faces (Figure 4A). SAED patterns show that these disordered dolomite crystals exhibit low-angle grain boundaries between neighboring nanocrystals. SAED patterns also show that Mg-silicate phases, confirmed by X-ray EDS spectra, do not have any diffraction peaks thereby indicating that these are amorphous phases (Supplemental figure 2). HAADF and X-ray EDS spectroscopic imaging demonstrate that disordered dolomite crystals are surrounded by amorphous Mg-silicate (Figure 4B & 4C).

Adsorption

Eighteen experiments were performed to quantify silica adsorption by calcite and dolomite with initial silica concentrations ranging from 0.5 mM to 1.4 mM. A control experiment using a solution with no calcite/dolomite seeds was performed to test the effect of the polyethylene bottles on the adsorption measurement. The control experiment resulted in an insignificant amount of adsorption or precipitation of amorphous silica on the bottle, consistent with results from Tutolo and Tosca (2018). The adsorption experiments showed that significant amounts of

dissolved silica are adsorbed onto both calcite and dolomite seeds (Figure 5). With increasing dissolved silica in solution, an increasing amount of silica was adsorbed onto calcite and dolomite (Figure 4). Adsorbed silica increased from ~21 μmol/m^2 (~13 molecules/nm^2) on calcite and ~7 μmol/m^2 (~4 molecules/nm^2) on dolomite with 0.5 mM in the solution to ~260 μmol/m^2 (~157 molecules/nm^2) on calcite and ~176 μmol/m^2 (~106 molecules/nm^2) on dolomite with 1.5 mM dissolved silica in the solution. Dolomite had slightly less adsorbed silica than calcite with 1 mM to 1.5 mM dissolved silica in the solution.

DISCUSSION

Many authors have demonstrated a positive correlation between microbial activity and sedimentary dolomite formation (Compton 1988; Hardie 1987, etc) and there has been extensive work performed on models of microbially mediated dolomite precipitation (Braissant et al. 2003; Kawano and Hwang 2011; Zhang et al. 2012b, 2015, 2021; Huang et al. 2019). However, an abiotic dolomite precipitation mechanism has not been well developed. Only a few attempts have been made to synthesis dolomite abiotically at low temperature. Earlier experiments, using more than 10 times the concentrations of Ca^{2+}, Mg^{2+} and CO_3^{2-} in seawater have produced Ca-Mg carbonates either with lower $MgCO_3$ content or as a hydrous phase (Glover and Sippel 1967; Devery and Ehlmann 1981; Kelleher and Redfern 2002; Schmidt et al. 2005). Using dissolved sulfide with a near modern seawater Mg:Ca ratio to synthesize dolomite instead has shown that precipitation of high magnesium calcite and disordered dolomite is possible at low temperature (Zhang et al. 2012a). Pseudo-hexagonal (001) surfaces of clay minerals and hematite have also been shown to promote the heterogeneous nucleation of calcite and high magnesian calcite, and to inhibit aragonite formation (Xu et al. 2018). Low temperature abiotic synthesis with addition of smectite has also resulted in the precipitation of disordered dolomite (Liu et al. 2019).

Synthesis with carboxylated polystyrene has been shown to promote aragonite growth but not dolomite precipitation (Roberts et al. 2013). On the other hand, many studies have recognized the relationship between abiotic dolomite and clays in various geologic settings (Polyak and Güven 2000; Díaz-Hernández et al. 2013; Wanas and Sallam 2016; Fang and Xu 2018).

Dissolved silica promotes disordered dolomite precipitation

In vitro experiments in this study demonstrate that dissolved silica can promote disordered dolomite precipitation at surface temperature in a seawater-like solutions. Subsequent mineralogical analyses reported here confirm the composition of the precipitates as Ca-Mg carbonate within the dolomite composition range while also exhibiting no cation ordering, conditions which we have defined in this study as being characteristic of disordered dolomite. The catalytic effect of the dissolved silica on disordered dolomite is two-fold: first, the presence of dissolved silica promotes the nucleation of the calcite-structure, and secondly, the adsorbed silica reduces the dehydration energy barrier of Mg-water surface complex and subsequently enhances Mg incorporation into the carbonate and promotes dolomite growth. At the same time, the presence of dissolved silica inhibits the formation of aragonite. Presence of minor amount of aragonite depositing on the exterior of disordered dolomite spherulite suggesting the aragonite likely formed after Mg-silicate formation reduced the dissolved silica concentration in solution. Further studies on the exact functional role of dissolved silica on Mg^{2+}-water dehydration warrants further investigation.

$Si(OH)_4$ is the predominant species of dissolved silica in circumneutral to slightly basic solutions, such as seawater (Applin 1987). Previous studies demonstrated that dissolved silica could promote calcite nucleation and inhibit aragonite formation by lowering the calcite nucleation energy (Kitano et al. 1979; Lakshtanov and Stipp 2010). When the dissolved silica concentration

exceeded saturation, aragonite was shown to be specifically inhibited with calcite being the dominant phase crystallized from Mg-free solutions (Lakshtanov and Stipp, 2010). It is likely that dissolved silica also lowers the nucleation energy of the Ca-Mg carbonates with calcite structures in this study. As the silica concentration in the solution increased, less aragonite and more disordered dolomite precipitated (Figure 1). Previous studies have indicated that silica polymerization occurs even when the solution concentration is below saturation (Iler 1975; Alvarez and Sparks 1985; Christl et al. 2012), and some have suggested that silica polymers or clusters can promote the formation of the calcite structure by creating new nucleation sites and by inhibiting formation of other carbonate polymorphs (Lakshtanov and Stipp, 2010). This study reports a similar effect whereby dissolved silica promotes the nucleation of Mg-calcite and disordered dolomite in Mg-bearing solutions. The dissolved silica appears to promote the nucleation of disordered dolomite by stabilizing calcite nuclei over those of aragonite (Lakshtanov and Stipp, 2010). It is also likely that the hexagon-like unit in the amorphous silica, similar to the six-membered silicate rings in opal-A and silica gel (Lee et al. 2020), may act similarly to mica by promoting the heterogeneous nucleation of Mg-calcite and disordered dolomite (Xu et al. 2018). Therefore, the presence of dissolved silica in the solution could enhance the nucleation of Mg-calcite and disordered dolomite.

This study also shows that adsorbed $Si(OH)_4$ can promote incorporation of Mg into the Ca-Mg carbonate phase. Although these experiments have slightly higher pH than seawater through most of geologic time (Halevy and Bachan 2017), the speciation of silica in this study is consistent with that inferred for paleo-seawater based on pH (Applin 1987). An increased concentration of dissolved silica was correlated with an increased mol.% of $MgCO_3$ in the disordered dolomite, especially at lower Mg:Ca ratios (Figure 2). Along similar lines, a recent

study has also recognized that the addition of dissolved silica could significantly enhance Mg incorporation into the Mg-bearing carbonates (Hobbs and Xu 2019). Previous studies with hydrogen sulfide, polysaccharides, and EPS have demonstrated that adsorbed substances can disrupt surface hydration layers and consequently promote Mg incorporation (Shen et al., 2014; Shen et al., 2015). Similarly, we propose that adsorbed silica can disturb the surface Mg-water complex and enhance surface dehydration, allowing the carbonate group (CO_3^{2-}) to bond with Mg cations on the crystal surface. The addition of low dipole moment substances, such as H_2S and methane can change the behavior of the solution, disrupt the surface Mg^{2+}-water complex, and promote disordered dolomite growth (Meister et al. 2007; Xu 2010; Zhang et al. 2012a, 2013). The low dipole moment $Si(OH)_4$ may have a similar effect on the Mg-water surface complex as other low dipole moment solutes.

Our results also show that a higher initial Mg:Ca ratio in the solution results in a higher $MgCO_3$ content within the synthetic Ca-Mg carbonates, which is consistent with previous studies (Hardie 1987; Zhang et al. 2012b, 2015). Further, the dumbbell-shaped, spherical aggregates with nanometer-sized crystals are similar to previous syntheses of disordered dolomite (Figure 3; Raz et al., 2000; Zhang et al., 2012; Zhang et al., 2015). The preferred orientation with low-angle grain boundaries between the Ca-Mg carbonate nano-crystals fits with the classical theory that the crystals grow randomly, but associate with less than <10° grain boundaries to minimize the interfacial energy (Dunn and Lionetti 1949; Read and Shockley 1950). Formation of these spherulites indicates the solutions are far from equilibrium (Gránásy et al. 2005).

The adsorption experiments show that a significant amount of silica can be adsorbed onto calcite and dolomite surfaces (Figure 4). The amount of adsorbed silica is consistent with previous experimental studies that demonstrated silica removal from solution during carbonate

precipitation (Kitano et al. 1979; Okumura et al. 1983; Tutolo and Tosca 2018). However, the exact role of the dissolved silica adsorption on promoting disordered dolomite precipitation is unknown and requires further study. A previous study on $SrCO_3$ precipitation suggested that spherulite and dumbbell morphologies are affected by solution pH and adsorbed silica may create new nucleation sites (Terada et al. 2003). The HAADF images obtained in this study show that synthetic disordered dolomite is similarly surrounded by amorphous Mg-silicate. It is interesting to note that XRD patterns show an elevated background (broad hump ranging from 8° to 10°) on the low angle side in both the 20 and 40°C syntheses. High dissolved silica and magnesium concentrations may have resulted in precipitation of amorphous Mg-bearing silicate (Figure 3). The elevated temperature (40°C) experiments show a narrower hump than the 20°C experiments indicating a slightly higher degree of crystallinity at higher temperature. Many studies have shown that the presence of Mg-silicate can promote precipitation of calcite and sometimes dolomite. Based on the morphology and textural relationship between carbonate and Mg-silicate in the early Cretaceous lacustrine carbonate, Wright and Barnett (2015) proposed that Mg-silicate precipitation may have triggered calcite nucleation and spherulite growth. Barium and strontium carbonate were observed in an alkaline lake water with an elevated silica concentration (García-Ruiz 1998). Tosca et al. (2011) demonstrated that elevated levels of SiO_2 and Mg^{2+} in a brine with similar salinity to modern seawater at pH > 8.7 could result in the formation of a Mg-silicate phase with a talc-like structure. Here, Mg-silicate may have acted as a template for heterogeneous nucleation similar to the role of mica in promoting Mg-calcite nucleation reported in a previous study (Xu et al. 2018). Therefore, the dissolved silica likely serves two roles in the formation of disordered dolomite: (1) dissolved silica and precipitated Mg-silica gel promote the nucleation of calcite and disordered dolomite; and (2) the low dipole

moment of the dissolved silica ($Si(OH)_4$) effectuates the dehydration of Mg^{2+}-water surface complexes enabling continuous growth of disordered dolomite.

Sedimentary dolomite as a paleoenvironment proxy

The relatively restricted range of silica and magnesium concentrations for which disordered dolomite precipitation has been demonstrated by this study implies that primary dolomite could be used as a proxy to interpret paleo-seawater composition. Due to the widespread occurrence of diatoms in marine environments, modern surface seawater is depleted in dissolved silica relative to paleo-ocean (Kidder and Tomescu 2016). Modern surface seawater generally has low dissolved silica, less than 40 μM (Abe and Watanabe 1992), and carbonate precipitation is dominated by aragonite with a minor amount of calcite despite the fact that seawater is saturated with respect to dolomite. However, primary dolomite has been reported in Deep Springs Lake, California (Meister et al. 2011; Hobbs and Xu 2019), and the Coorong region, South Australia (Rosen et al. 1988). These hypersaline dolomitic lakes are concentrated in Ca, Mg, and dissolved silica (Jones et al. 1967), at levels similar to the concentrations used in this study and provide points of reference for Proterozoic and Early Paleozoic seawater with respect to silica and magnesium. Muir et al. (1980) pointed out that carbonate in the Coorong region is accompanied by chert formation which indicates silica concentrations might be close to saturation with respect to amorphous silica. Some of the hypersaline lakes with modern dolomite precipitation summarized by Last (1990) have relatively high concentrations of dissolved silica. Our syntheses and several modern dolomite-forming lakes provide constraints on the conditions required for abiotic dolomite precipitation (Figure 6). This activity-activity diagram can be used to infer the possibility of primary dolomite precipitation on the basis of solution chemistry. One study has shown that groundwater hosted within weathering basalt and concentrated in Mg and silica in

Amboseli, Kenya resulted in precipitation of dolomite, kerolite and sepiolite (Stoessell and Hay 1978). The groundwater flowing through the Pleistocene sediments show dissolved silica concentrations from 0.2 mM to 2 mM where all sites with dolomite have dissolved silica concentration higher than 1 mM (Stoessell and Hay 1978). Studies at elevated pH (pH > 9.5) show Mg-silicate precipitation occurs alongside calcite rather than dolomite (Wright and Barnett 2015; Mercedes-Martín et al. 2016, 2017; Tutolo and Tosca 2018). When pH increases to more than 9.5, the dominant silica species changes from the neutral $Si(OH)_4$ to $SiO(OH)_3^-$ and $Si_2O_3(OH)_4^{2-}$ (Applin 1987). These negatively charged dissolved silica species act to remove Mg^{2+} from the solution by bonding with magnesium and forming amorphous Mg-silicate, which may later transform to Mg-silicate clay. This process effectively depletes Mg in the solution and results in calcite precipitation over dolomite. These model environments suggest natural settings with pH lower than 9.5 and high concentrations of dissolved silica and magnesium could result in dolomite precipitation.

Many studies have documented that dolomite and calcite are often associated with stratiform or nodular chert, especially within the older rock record (Walker, 1962; Muir et al., 1980; Maliva et al., 1989; Maliva et al., 2005; Bustillo, 2010). Siever (1992) suggested dissolved silica in Precambrian seawater was controlled mainly by amorphous silica saturation (~1.8 mM) prior to the presence of silica-consuming microorganisms. The lower bound of dissolved silica for the majority of Proterozoic is suggested to be around 1.3 mM considering the interaction between iron oxide and silica (Conley et al. 2017). At the end of the Neoproterozoic, siliceous organisms such as sponges and radiolarians appeared and increased the removal of dissolved silica from seawater (Maliva et al., 1989; Conley et al., 2017). From the Late-Neoproterozoic to Mid-Mesozoic, dissolved silica concentrations in seawater are estimated to have ranged from ~ 0.5

377 mM (Conley et al. 2017) to ~ 1 mM (Siever 1991). Our abiotic dolomite precipitation model
378 suggests that a significant volume of primary sedimentary dolomite from the Precambrian
379 supereon and most of the Phanerozoic eon might have precipitated from the catalytic effect of
380 dissolved silica in silica-rich seawater. The reported dissolved silica level from the Proterozoic to
381 early Mesozoic is sufficient to catalyze disordered dolomite formation based on our results. Both
382 Siever (1991) and Conley et al. (2017) provide general trends for silica concentrations in paleo-
383 seawater. However, smaller timescale oscillations have not been reported. This study suggests
384 that it may be possible to use large scale primary dolomite abundance, such as Macrostrat data,
385 as a proxy to understand the changes in marine silica concentration deep into the rock record
386 (with careful consideration of the effects of diagenesis and microbial involvement).

387 **IMPLICATIONS**

388 The appearance of diatoms in the Mesozoic greatly impacted the biogeochemical cycle of Si and
389 resulted in the rapid decline in dissolved silica to the micro-molar concentrations observed in the
390 modern surface ocean (Figure 7; Maliva et al., 1989; Conley et al., 2017). To a first-order
391 approximation, the dissolved silica in seawater from Siever (1991) and Conley et al. (2017) is
392 positivity correlated with dolomite abundance in marine sediments (Figure 7). One prior study
393 has suggested that a transition from abiotic to biogenic control of calcite precipitation occurred in
394 the Jurassic (Eichenseer et al. 2019). A similar transition might have occurred for dolomite
395 precipitation as depletion of dissolved silica in seawater is also correlated with a decrease in the
396 extent of abiotic dolomite precipitation. The radiation of the diatoms, and the subsequent
397 decrease in the availability of dissolved silica coincided with the plummeting abundance in
398 sedimentary dolomite in the Mid-Cretaceous (Given and Wilkinson 1987). Further, the number
399 of diatom species increased by two orders of magnitude from ~60 Ma to the present day (Harper

and Knoll 1975). This evidence suggests that the diversification of diatoms has greatly impacted the formation of sedimentary dolomite by efficiently removing dissolved silica from seawater. The depletion of dissolved silica in the modern ocean by the effective extraction from diatoms might be responsible for the decline in primary dolomite formation.

Our results show that 1-2 mM dissolved silica can catalyze disordered dolomite precipitation at room temperature in seawater-like solutions. This new mechanism of silica-catalyzed dolomite formation has the ability to address an outstanding aspect of the "dolomite problem". This model can complement microbially catalyzed models and complete other previous abiotic dolomite models with added catalysts such as the evaporation pumping model (Hsu and Siegenthaler 1969) and the normal seawater model (Saller 1984). The dissolved silica concentration may be elevated in certain modern environments through aeolian inputs, evaporative pumping and evaporation in shallow lagoons with the input of dissolved silica-bearing groundwater from continent side. Moreover, based on the Ca-Mg carbonate formation conditions from this study, a model could be constructed to explain the dramatic shift in carbonate precipitation and predict ancient seawater Mg/Ca ratios and dissolved silica concentrations on the basis of large-scale compiled dolomite abundance from database. Our model also posits a new constraint on the appearance of silica-consuming microorganisms from the drastic change in dolomite abundance. Our results may provide new insights into the long-lasting cap carbonate (Hoffman et al. 1998) question, as recent work suggests a link between synchronized cap dolomite precipitation and a spike of dissolved silica input following the deglaciation of the Marinoan snowball earth (Penman and Rooney 2019). With the combination of high pCO_2 level coupled with an excess input of dissolved Ca, Mg and silica from deglaciation, our model predicts that dolomite could be readily formed and deposited in shallow sea environments. Our model allows a first-order

423 approximation for the composition of Proterozoic seawater conforming to massive dolomite
424 volume and tests different pCO_2, which are closely related to global tectonic activity, during the
425 Proterozoic Eon (Supplemental figure 3&4). This could potentially help to contextualize the
426 presence of the dolomitic diamictite and dolomitic sandstone and cap dolomite (Fairchild et al.
427 2016) formed before and after the Marinoan.

428 **ACKNOWLEDGEMENT**

429 We would like to thank Dr. Adam Wallace and the two anonymous reviewers for their
430 constructive comments and suggestions. We acknowledge NASA Astrobiology Institute and the
431 S.W. Bailey Fellowship of the Department of Geoscience, University of Wisconsin-Madison for
432 supporting this study.

433

434 **REFERENCES CITED**

435 Abe, K., and Watanabe, Y. (1992) Determination of silicate in seawater by inductively coupled
436 plasma atomic emission spectrometry. Journal of Oceanography, 48, 283–292.

437 Alvarez, R., and Sparks, D.L. (1985) Polymerization of silicate anions in solutions at low
438 concetnrations. Nature, 318, 649–651.

439 Applin, K.R. (1987) The diffusion of dissolved silica in dilute aqueous solution. Geochimica et
440 Cosmochimica Acta, 51, 2147–2151.

441 Applin, R. (1987) The diffusion of dissolved silica in dilute aqueous solution, 51, 2147–2151.

442 Awramik, S.M., and Sprinkle, J. (1990) Proterozoic stromatolites : The first marine evolutionary
443 biota. Historical Biology, 13, 241–253.

444 Barnes, I., and Back, W. (1964) Dolomite solubility in ground water in. In Short papers in
445 geology and hydrology Articles 122-172, Geological Survey Research 1963, Geological
446 survey professional paper 475-D pp. D179–D180. United States Government Printing
447 Office, Washington.

448 Berner, R.A. (1975) The role of magnesium in the crystal growth of calcite and aragonite from
449 sea water. Geochimica et Cosmochimica Acta, 39, 489–504.

450 Braissant, O., Cailleau, G., Dupraz, C., and Verrecchia, E.P. (2003) Bacterially induced
451 mineralization of calcium carbonate in terrestrial environments: the role of
452 exopolysaccharides and amino acids. Journal of Sedimentary Research, 73, 485–490.

453 Bustillo, M.A. (2010) Silicification of Continental Carbonates. Developments in Sedimentology,
454 62, 153–178.

455 Chahi, A., Fritz, B., Duplay, J., Weber, F., and Lucas, J. (1997) Textural transition and genetic
456 relationship between precursor stevensite and sepiolite in lacustrine sediments (Jbel
457 Rhassoul, Morocco). Clays and Clay Minerals, 45, 378–389.

458 Christl, I., Brechbühl, Y., Graf, M., and Kretzschmar, R. (2012) Polymerization of silicate on
459 hematite surfaces and its influence on arsenic sorption. Environmental Science and
460 Technology, 46, 13235–13243.

461 Clesceri, L.S., Greenberg, A.E., and Eaton, A.D. (1999) Standard methods for the exmination of
462 water and wastewater, 20th ed., 1325 p. American Public Health Association, Washington,
463 DC.

464 Compton, J.S. (1988) Degree of supersaturation and precipitation of organogenic dolomite.

Geology, 16, 318–321.

Conley, D.J., Frings, P.J., Fontorbe, G., Clymans, W., Stadmark, J., Hendry, K.R., Marron, A.O., and De La Rocha, C.L. (2017) Biosilicification Drives a Decline of Dissolved Si in the Oceans through Geologic Time. Frontiers in Marine Science, 4.

Curtis, R., Evans, G., Kinsman, D.J.J., and Shearman, D.J. (1963) Association of Dolomite and Anhydrite in the Recent Sediments of the Persian Gulf. Nature, 197, 679–680.

Devery, D.M., and Ehlmann, A.J. (1981) Morphological changes in a series of synthetic Mg-calcites. American Mineralogist, 66, 592–595.

Díaz-Hernández, J.L., Sánchez-Navas, A., and Reyes, E. (2013) Isotopic evidence for dolomite formation in soils. Chemical Geology, 347, 20–33.

Dunn, C.G., and Lionetti, F.G. (1949) The effect of orientation difference on grain boundary energies. Journal of Metals, 1, 125–132.

Eichenseer, K., Balthasar, U., Smart, C.W., Stander, J., Haaga, K.A., and Kiessling, W. (2019) Jurassic shift from abiotic to biotic control on marine ecological success. Nature Geoscience, 12.

Fairchild, I.J., Bonnand, P., Davies, T., Fleming, E.J., Grassineau, N., Halverson, G.P., Hambrey, M.J., McMillan, E.M., McKay, E., Parkinson, I.J., and others (2016) The Late Cryogenian Warm Interval, NE Svalbard: Chemostratigraphy and genesis. Precambrian Research, 281, 128–154.

Fang, Y., and Xu, H. (2018) Study of an Ordovician carbonate with alternating dolomite–calcite laminations and its implication for catalytic effects of microbes on the formation of

sedimentary dolomite. Journal of Sedimentary Research, 88, 679-695.

Fang, Y., and Xu, H. (2019) A new approach to quantify ordering state of protodolomite using XRD, TEM, and Z-contrast imaging. Journal of Sedimentary Research, 89, 537–551.

García-Ruiz, J.M. (1998) Carbonate precipitation into alkaline silica-rich environments. Geology, 26, 843–846.

Given, R.K., and Wilkinson, B.H. (1987) Dolomite abundance and stratigraphic age; constraints on rates and mechanisms of Phanerozoic dolostone formation. Journal of Sedimentary Research, 57, 1068–1078.

Glover, E.D., and Sippel, R.F. (1967) Synthesis of magnesium calcites. Geochimica et Cosmochimica Acta, 31, 603–613.

Gránásy, L., Pusztai, T., Tegze, G., Warren, J.A., and Douglas, J.F. (2005) Growth and form of spherulites. Physical Review E - Statistical, Nonlinear, and Soft Matter Physics, 72, 1–15.

Gregg, J.M., and Frank, T.D. (2009) Data report : dolomite in Neogene sediments of the Belgica carbonate mound province , Porcupine Seabight , North Atlantic 1, 307, 1–12.

Gregg, J.M., Bish, D.L., Kaczmarek, S.E., and Machel, H.G. (2015) Mineralogy, nucleation and growth of dolomite in the laboratory and sedimentary environment: A review. Sedimentology, 62, 1749–1769.

Halevy, I., and Bachan, A. (2017) The geologic history of seawater pH. Science, 355, 1069–1071.

Hardie, L. a (1987) Dolomitization; a critical view of some current views. Journal of Sedimentary Research, 57, 166–183.

Harper, H.E., and Knoll, A.H. (1975) Silica, diatoms, and Cenozoic radiolarian evolution.

507 Geology, 3, 175–177.

508 Hobbs, F.W.C., and Xu, H. (2019a) Magnesite formation through temperature and pH cycling as
509 a proxy for lagoon and playa paleoenvironments. Geochimica et Cosmochimica Acta.

510 Hoffman, P.F., Kaufman, A.J., Halverson, G.P., and Schrag, D.P. (1998) A Neoproterozoic
511 snowball earth. Science, 281, 1342–1346.

512 Hsu, K.J., and Siegenthaler, C. (1969) Preliminary Experiments on Hydrodynamic Movement
513 Induced By Evaporation and Their Bearing on the Dolomite Problem. Sedimentology, 12,
514 11–25.

515 Huang, Y., Yao, Q., Li, H., Wang, F., Zhou, G., and Fu, S. (2019) Aerobically incubated
516 bacterial biomass-promoted formation of disordered dolomite and implication for dolomite
517 formation Aerobically incubated bacterial biomass-promoted formation of disordered
518 dolomite and implication for dolomite formation. Chemical Geology, 523, 19–30.

519 Iler, R.K. (1975) Coagulation of Colloidal Silica by Calcium Ions , Mechanism , and Effect of
520 Particle Size. Journal of Colloid and Interface Science, 53, 476–488.

521 Jones, B.F., Rettig, S.L., and Eugster, H.P. (1967) Silica in alkaline brines. Science, 158, 1310–
522 1314.

523 Kaczmarek, S.E., Gregg J.M., Bish, D., Machel, H., and Fouke, B. (2017) Dolomite, very high-
524 magnesium calcite, and microbes—implications for the microbial model of dolomitization,
525 in Characeterization and Modeling of Carbonates - Mountjoy Symposium 1. In A. MacNeil,
526 J. Lonnee, and R. Wood, Eds., SEPM Special Publication Vol. 109, p. 17.

527 Kawano, M., and Hwang, J. (2011) Roles of microbial acidic polysaccharides in precipitation

528 rate and polymorph of calcium carbonate minerals. Applied Clay Science, 51, 484–490.

529 Kelleher, I.J., and Redfern, S.A.T. (2002) Hydrous calcium magnesium carbonate, A possible
530 precursor to the formation of sedimentary dolomite. Molecular Simulation, 28, 557–572.

531 Kendall, G.S.C., and Skipwith, P.A. d'E. (1968) Recent algal mats of a Persian Gulf lagoon.
532 Journal of Sedimentary Research, 38, 1040–1058.

533 Kidder, D.L., and Tomescu, I. (2016) Biogenic chert and the Ordovician silica cycle.
534 Palaeogeography, Palaeoclimatology, Palaeoecology, 458, 29–38.

535 Kitano, Y., Okumura, M., and Idogaki, Masatoshi, 1979 (1979) Behavior of dissolved silica in
536 parent solution at the formation of calcium carbonate, 13, 253–260.

537 Lakshtanov, L.Z., and Stipp, S.L.S. (2010) Interaction between dissolved silica and calcium
538 carbonate: 1. Spontaneous precipitation of calcium carbonate in the presence of dissolved
539 silica. Geochimica et Cosmochimica Acta, 74, 2655–2664.

540 Land, L.S. (1980) The isotopic and trace element geochemistry of dolomite: the state of the art.
541 Concepts and Models of Dolomization:SEPM, Special Publication, 28, 87–110.

542 Land, L.S. (1998) Failure to precipitate dolomite at 25°C from dilute solution despite 1000-fold
543 oversaturation after 32 years. Aquatic Geochemistry, 4, 361–368.

544 Last, W.M. (1990) Lacustrine dolomite-an overview of modern, Holocene, and Pleistocene
545 occurrences. Earth Science Reviews, 27, 221–263.

546 Lee, S., Cai, J., Jin, S., Zhang, D., Thevamaran, R., and Xu, H. (2020) Coesite Formation at Low
547 Pressure during Supersonic Microprojectile Impact of Opal. ACS Earth and Space
548 Chemistry, 4, 1291–1297.

549 Lippmann, F. (1973) The Polymorphism Calcite-Aragonite. In Sedimentary Carbonate Minerals.
550 Springer, New York.

551 Liu, D., Xu, Y., Papineau, D., Yu, N., Fan, Q., Qiu, X., and Wang, H. (2019) Experimental
552 evidence for abiotic formation of low-temperature proto-dolomite facilitated by clay
553 minerals. Geochimica et Cosmochimica Acta, 247, 83–95.

554 Lu, Y., Sun, X., Xu, H., Konishi, H., Lin, Z., Xu, L., Chen, T., Hao, X., Lu, H., and Peckmann, J.
555 (2018) Formation of dolomite catalyzed by sulfate-driven anaerobic oxidation of methane :
556 Mineralogical and geochemical evidence from the northern South China Sea, 103, 720–734.

557 Lumsden, D.N. (1988) Characteristics of Deep-Marine Dolomite, 58, 2–10.

558 Maliva, R.G., Knoll, A.H., and Siever, R. (1989) Secular Change in Chert Distribution: A
559 Reflection of Evolving Biological Participation in the Silica Cycle. Palaios, 4, 519.

560 Maliva, R.G., Knoll, A.H., and Simonson, B.M. (2005) Secular change in the Precambrian silica
561 cycle: Insights from chert petrology. Bulletin of the Geological Society of America, 117,
562 835–845.

563 Meister, P., Mckenzie, J.A., Vasconcelos, C., Sconi, S.B., Frank, M.A., Gutjahr, M., and Schrag,
564 D.A.P. (2007) Dolomite formation in the dynamic deep biosphere : results from the Peru
565 Margin. Sedimentology, 1007–1031.

566 Meister, P., Reyes, C., Beaumont, W., Rincon, M., Collins, L., Berelson, W., Stott, L., Corsetti,
567 F., and Nealson, K.H. (2011) Calcium and magnesium-limited dolomite precipitation at
568 Deep Springs Lake, California. Sedimentology, 58, 1810–1830.

569 Mercedes-martín, R., Rogerson, M.R., Brasier, A.T., Vonhof, H.B., Prior, T.J., Fellows, S.M.,

570 Reijmer, J.J.G., Billing, I., and Pedley, H.M. (2016) Growing spherulitic calcite grains in
571 saline , hyperalkaline lakes : experimental evaluation of the effects of Mg-clays and organic
572 acids. Sedimentary Geology, 335, 93–102.

573 Mercedes-Martín, R., Brasier, A.T., Rogerson, M., Reijmer, J.J.G., Vonhof, H., and Pedley, M.
574 (2017) A depositional model for spherulitic carbonates associated with alkaline , volcanic
575 lakes. Marine and Petroleum Geology, 86, 168–191.

576 Morey, G.W. (1962) The action of water on calcite, magnesite and dolomite. American
577 Mineralogist: Journal of Earth and Planetary Materials, 47, 1456–1460.

578 Mucci, A., and Morse, J.W. (1983) The incorporation of Mg2+ and Sr2+ into calcite
579 overgrowths: influences of growth rate and solution composition. Geochimica et
580 Cosmochimica Acta, 47, 217–233.

581 Muir, M., Lock, D., and Von Der Borch, C. (1980) The Coorong model for
582 penecontemporaneous dolomite formation in the Middle Proterozoic McArthur Group,
583 Northern Territory, Austrailia. SEPM Special Publication, 28, 51–67.

584 Okumura, M., Kitano, Y., and Idogaki, M. (1983) Removal of anions by carbonate from
585 seawater sedimentation, 17, 105–110.

586 Oomori, T., and Kitano, Y. (1987) Synthesis of protodolomite from sea water containing dioxane.
587 Geochemical Journal, 21, 59–65.

588 Penman, D.E., and Rooney, A.D. (2019) Coupled carbon and silica cycle perturbations during
589 the Marinoan snowball Earth deglaciation. Geology.

590 Peters, S.E., Husson, J.M., and Wilcots, J. (2017) The rise and fall of stromatolites in shallow

591 marine environments. Geology, 45, 487–490.

592 Peterson, M.N.A., Bien, G.S., and Berner, R.A. (1963) Radiocarbon studies of recent dolomite
593 from Deep Springs Lake, California. Journal of Geophysical Research, 68, 6493–6505.

594 Polyak, V.J., and Güven, N. (2000) Authigenesis of trioctahedral smectite in magnesium-rich
595 carbonate speleothems in Carlsbad Cavern and other caves of the Guadalupe Mountains,
596 New Mexico. Clays and Clay Minerals, 48, 317–321.

597 Raz, S., Weiner, S., and Addadi, L. (2000) Formation of high-magnesian calcites via an
598 amorphous precursor phase: possible biological implications. Advanced Materials, 12, 38–
599 42.

600 Read, W.T., and Shockley, W. (1950) Dislocation models of crystal grain boundaries. Physical
601 Review, 78.

602 Roberts, J.A., Kenward, P.A., Fowle, D.A., Goldstein, R.H., González, L.A., and Moore, D.S.
603 (2013) Surface chemistry allows for abiotic precipitation of dolomite at low temperature.
604 Proceedings of the National Academy of Sciences, 110, 14540–14545.

605 Rosen, M.R., Miser, D.E., and Warren, J.K. (1988) Sedimentology, mineralogy and isotopic
606 analysis of Pellet Lake, Coorong region, South Australia. Sedimentology, 35, 105–122.

607 Saller, A.H. (1984) Petrologic and geochemical constraints on the origin of subsurface dolomite,
608 Enewetak Atoll: an example of dolomitization by normal seawater (Eocene, Sr-isotopes).
609 Geology, 12, 217–220.

610 Schmidt, M., Xeflide, S., Botz, R., and Mann, S. (2005) Oxygen isotope fractionation during
611 synthesis of CaMg-carbonate and implications for sedimentary dolomite formation.

612 Geochimica et Cosmochimica Acta, 69, 4665–4674.

613 Shen, Z., Liu, Y., Brown, P.E., Szlufarska, I., and Xu, H. (2014) Modeling the Effect of
614 Dissolved Hydrogen Sulfide on Mg 2+ –Water Complex on Dolomite {104} Surfaces. The
615 Journal of Physical Chemistry C, 140710065446006.

616 Shen, Z., Szlufarska, I., Brown, P.E., and Xu, H. (2015) Investigation of the Role of
617 Polysaccharide in the Dolomite Growth at Low Temperature by Using Atomistic
618 Simulations. Langmuir, 31, 10435–10442.

619 Sibley, D.F., Nordeng, S.H., and Borkowski, M.L. (1994) Dolomitization kinetics of
620 hydrothermal bombs and natural settings. Journal of Sedimentary Research, 64, 630–637.

621 Siever, R. (1991) Silica in the oceans: Biological-Geochemical Interplay. In S.H. Schneider and
622 P.J. Boston, Eds., Scientists on Gaia pp. 287–295. MIT Press, Cambridge, Massachusetts.

623 ——— (1992) The silica cycle in the Precambrian. Geochimica et Cosmochimica Acta, 56,
624 3265–3272.

625 Stanley, S.M., Ries, J.B., and Hardie, L.A. (2002) Low-magnesium calcite produced by coralline
626 algae in seawater of Late Cretaceous composition. Proc Natl Acad Sci U S A, 99, 15323–
627 15326.

628 Stoessell, R.K. (1988) 25°C and 1 atm dissolution experiments of sepiolite and kerolite.
629 Geochimica et Cosmochimica Acta, 52, 365–374.

630 Stoessell, R.K., and Hay, R.L. (1978) The geochemical origin of sepiolite and kerolite at
631 Amboseli. Contributions to MIneralogy and Petrology, 65, 255–267.

632 Stout, J.W., and Robie, R.A. (1963) Heat capacity from 11 to 300°K., entropy, and heat of

633 formation of dolomite. Journal of Physical Chemistry, 67, 2248–2252.

634 Terada, T., Yamabi, S., and Imai, H. (2003) Formation process of sheets and helical forms
635 consisting of strontium carbonate fibrous crystals with silicate. Journal of Crystal Growth,
636 253, 435–444.

637 Tosca, N.J., Macdonald, F.A., Strauss, J. V., Johnston, D.T., and Knoll, A.H. (2011)
638 Sedimentary talc in Neoproterozoic carbonate successions. Earth and Planetary Science
639 Letters, 306, 11–22.

640 Tutolo, B.M., and Tosca, N.J. (2018) Experimental examination of the Mg-silicate-carbonate
641 system at ambient temperature: Implications for alkaline chemical sedimentation and
642 lacustrine carbonate formation. Geochimica et Cosmochimica Acta, 225, 80–101.

643 Vasconcelos, C., and McKenzie, J.A. (1997) Microbial mediation of modern dolomite
644 precipitation and diagenesis under anoxic conditions (Lagoa Vermelha, Rio de Janeiro,
645 Brazil). Journal of sedimentary Research, 67, 378–390.

646 Walker, T.R. (1962) Reversible nature of chert-carbonate replacement in sedimentary rocks.
647 Geological Society of America Bulletin, 73, 237–242.

648 Wanas, H.A., and Sallam, E. (2016) Abiotically-formed, primary dolomite in the mid-Eocene
649 lacustrine succession at Gebel El-Goza El-Hamra, NE Egypt: An approach to the role of
650 smectitic clays. Sedimentary Geology, 343, 132–140.

651 Warren, J. (2000) Dolomite: occurrence, evolution and economically important associations.
652 Earth-Science Reviews, 52, 1–81.

653 Wright, D.T., and Wacey, D. (2005) Precipitation of dolomite using sulphate-reducing bacteria

654 from the Coorong Region, South Australia: significance and implications. Sedimentology,
655 52, 987–1008.

656 Wright, V.P., and Barnett, A.J. (2015) An abiotic model for the development of textures in some
657 South Atlantic early Cretaceous lacustrine carbonates Cretaceous. Geological Society,
658 London, Special Publications, 418, 1–11.

659 Xiong, Y. (2008) Thermodynamic properties of brucite determined by solubility studies and their
660 significance to nuclear waste isolation. Aquatic Geochemistry, 14, 223–238.

661 Xu, H. (2010) Synergistic roles of microorganisms in mineral precipitates acssociated with deep
662 sea methane seeps. In Geomicrobiology: Molecular and Environmental Perspective2 pp.
663 325–346.

664 Xu, H., Zhou, M., Fang, Y., and Teng, H.H. (2018) Effect of Mica and Hematite (001) Surfaces
665 on the Precipitation of Calcite. Minerals, 8.

666 Zhang, F., Xu, H., Konishi, H., and Roden, E.E. (2010) A relationship between d104 value and
667 composition in the calcite-disordered dolomite solid-solution series. American Mineralogist,
668 95, 1650–1656.

669 Zhang, F., Xu, H., Konishi, H., Kemp, J.M., Roden, E.E., and Shen, Z. (2012a) Dissolved
670 sulfide-catalyzed precipitation of disordered dolomite: Implications for the formation
671 mechanism of sedimentary dolomite. Geochimica et Cosmochimica Acta, 97, 148–165.

672 Zhang, F., Xu, H., Konishi, H., Shelobolina, E.S., and Roden, E.E. (2012b) Polysaccharide-
673 catalyzed nucleation and growth of disordered dolomite: A potential precursor of
674 sedimentary dolomite. American Mineralogist, 97, 556–567.

675 Zhang, F., Yan, C., Teng, H.H., Roden, E.E., and Xu, H. (2013) In situ AFM observations of Ca-
676 Mg carbonate crystallization catalyzed by dissolved sulfide: Implications for sedimentary
677 dolomite formation. Geochimica et Cosmochimica Acta, 105, 44–55.

678 Zhang, F., Xu, H., Shelobolina, E.S., Konishi, H., Converse, B., Shen, Z., and Roden, E.E. (2015)
679 The catalytic effect of bound extracellular polymeric substances excreted by anaerobic
680 microorganisms on Ca-Mg carbonate precipitation: Implications for the "dolomite problem."
681 American Mineralogist, 100, 483–494.

682 Zhang, F., Xu, H., Shelobolina, E.S., Konishi, H., and Roden, E.E. (2021) Precipitation of low-
683 temperature disordered dolomite induced by extracellular polymeric substances of
684 methanogenic Archaea *Methanosarcina barkeri***:** Implications for sedimentary dolomite
685 formation. American Mineralogist (in press).

686

687

688 **Figure caption**

689 Figure 1. XRD pattern of synthetic Ca-Mg carbonate grown with 1 mM and 2mM dissolved
690 silica at (A) 20°C and (C) 40°C with initial solution [Mg]:[Ca] = 3:1 and 5:1. (B) Zoom-in XRD
691 pattern around the (104) peaks of disordered dolomite showing changes in unit cell parameters.
692 D = disordered dolomite, A = aragonite, respectively. In all patterns, the red line indicates fitting
693 from refinement and the black line at the bottom indicates residue. The disctinction between
694 high-magnesium calcite and disordered dolomite at 36 mol.% $MgCO_3$ (corresponding to d_{104} =
695 2.948 Å, $2\theta = 13.82°$) is chosen based on modern protodolomite (Fang and Xu 2019).

696

697 Figure 2. The mole percent of $MgCO_3$ in the solid phase vs. [Mg]:[Ca] ratio in solution.
698 Dissolved silica showed a significant catalytic effect on Mg^{2+}-water dehydration and subsequent
699 incorporation into the carbonate structure. The divide of high-magnesium calcite and disordered
700 dolomite at 36 mol.% $MgCO_3$ (corresponding to d_{104} = 2.948 Å, $2\theta = 13.82°$) is chosen based on
701 modern protodolomite (Fang and Xu 2019). Coralline algae and control were constructed with
702 Stanley et al. (2002), and Mucci and Morse (1983), respectively.

703

704 Figure 3. (A) BSE image of disordered dolomite spherulites synthesized at 20 °C with 2 mM of
705 dissolved silica and an initial Mg:Ca ratio of 5:1. BSE image of (B) disordered dolomite
706 spherulites and (C) Mg-silicate synthesized at 40 °C with 2 mM of dissolved silica and an initial
707 Mg:Ca ratio of 5:1. The X-ray EDS spectra from the disordered dolomite and Mg-silicate are
708 inserted at the lower-right corner of each image.

709

Figure 4. (A) A bright-field TEM image of disordered dolomite nano-crystals. Diffraction arcs indicate disordered dolomite nanocrystals behave similarly to single crystal diffraction with low-angle grain boundaries present (inserted at lower-right corner). An X-ray EDS spectrum from the crystal is also inserted at the upper-right corner. (B) HAADF image of disordered dolomite surrounded by Mg-silicate gel. (C) XEDS elemental mapping showing Mg, Ca and Si distribution in the same area as HAADF image.

Figure 5. Adsorbtion of dissolved silica onto calcite chalk and a chalk-like micro-dolomite samples.

Figure 6. Activity-activity diagram for solutions that may exist in dolomite forming environments. The solubility curves of the various mineral phases are based on the *log K* values for the mineral solubility reaction with fixed pH = 8.5, $[Ca^{2+}]$ = 10 mM, and fixed $[CO_2]$ = 400 ppm at 25°C. The pink area indicates possible water conditions for dolomite formation and the possible Proterozoic seawater silica and Mg concentrations. The blue dotted circle is a possible Proterozoic seawater range based on the formation of dolomite and assumed near saturation with respect to dissolved silica. Deep Springs Lake (DSL) in California (Jones et al. 1967), Pellet Lake, and Milne Lake in Australia (Wright and Wacey 2005), and groundwater at Amboseli, Kenya (Stoessell and Hay, 1978) are plotted based on published work and provide examples of environments with modern dolomite. Mineral *log* K values were obtained from various reference listed below: brucite (Xiong 2008), disordered dolomite (Stout and Robie 1963), dolomite

732 (Barnes and Back 1964), kerolite (Stoessell 1988), magnesite (Morey 1962), sepiolite
733 (PHREEQC), sepiolite (amorphous) (PHREEQC), stevensite (Chahi et al. 1997), talc
734 (PHREEQC),

735

736 Figure 7. Changes in dolomite and dissolved silica from the Mesozoic (220 Ma) to the present.
737 The percent of dolomite indicates the percentage of dolomite in sedimentary carbonate. Siever
738 (1991) and Conley et al. (2017) provided upper and lower bounds for dissolved silica. The red
739 star is based on Conley et al. (2017).

Table 1. Synthesis conditions and refinement results of the products.

	Conditions					**Saturation index**			**Phase Fraction**				**Unit cell parameters of dolomite/ calcite**			
Sample #	[Si]	Mg:Ca	Starting pH	End pH	Temp (°C)	Dol.	Cal.	Arag.	Dol.	Cal.	Arag.	Hyd..	*a* (Å)	*c* (Å)	d_{104} (Å)	Mole % of $MgCO_3$% in Ca-Mg carbonate
1	1mM	3:1	8.93	8.85	20	4.50	1.96	1.82	53.6	-	46.4	-	4.892(3)	16.599(15)	2.956	32.4 ± 1.1
2	2mM		8.96	8.87		4.89	2.15	2.01	35.8	-	64.2	-	4.879(6)	16.526(19)	2.948	37.1 ± 1.9
3	1mM	5:1	8.88	8.67		4.53	1.87	1.72	49.1	-	50.9	-	4.861(8)	16.500(27)	2.939	41.9 ± 2.7
4	2mM		8.86	8.64		4.91	2.06	1.91	40.7	-	59.3	-	4.853(3)	16.434(21)	2.927	48.7 ± 1.6
5	1mM	3:1	8.91	8.75	40	4.53	1.87	1.74	40.0	-	60.0	-	4.889(3)	16.577(12)	2.956	32.3 ± 1.0
6	2mM		8.87	8.79		4.59	2.03	1.89	75.1	-	24.9	-	4.880(5)	16.543(21)	2.954	33.8 ± 1.8
7	1mM	5:1	9.15	8.55		4.58	1.79	1.65	47.3	-	29.1	23.6	4.845(4)	16.423(23)	2.935	43.9 ± 2.0
8	2mM		9.17	8.62		4.90	1.94	1.81	63.4	-	33.1	3.6	4.847(4)	16.373(21)	2.931	44.9 ± 1.9
Control 1	0 mM	3:1	8.64	8.46	20	3.99	1.71	1.57	-	2.6	97.4	-	4.989(4)	16.862(23)	3.017	6.2 ± 1.0
Control 2	0 mM	5:1	8.46	8.27	20	4.02	1.61	1.47	-	2.9	97.1	-	4.984(4)	16.702(21)	3.012	8.1 ± 1.1

Dol. = dolomite, Cal. = calcite, Arag. = aragonite, Hyd. = hydromagnesite. Saturation index = log (IAP/K_{sp}), where IAP = ion activity product and K_{sp} = solubility product.

This is the peer-reviewed, final accepted version for American Mineralogist, published by the Mineralogical Society of America.
The published version is subject to change. Cite as Authors (Year) Title. American Mineralogist, in press.
DOI: https://doi.org/10.2138/am-2021-7474. http://www.minsocam.org/

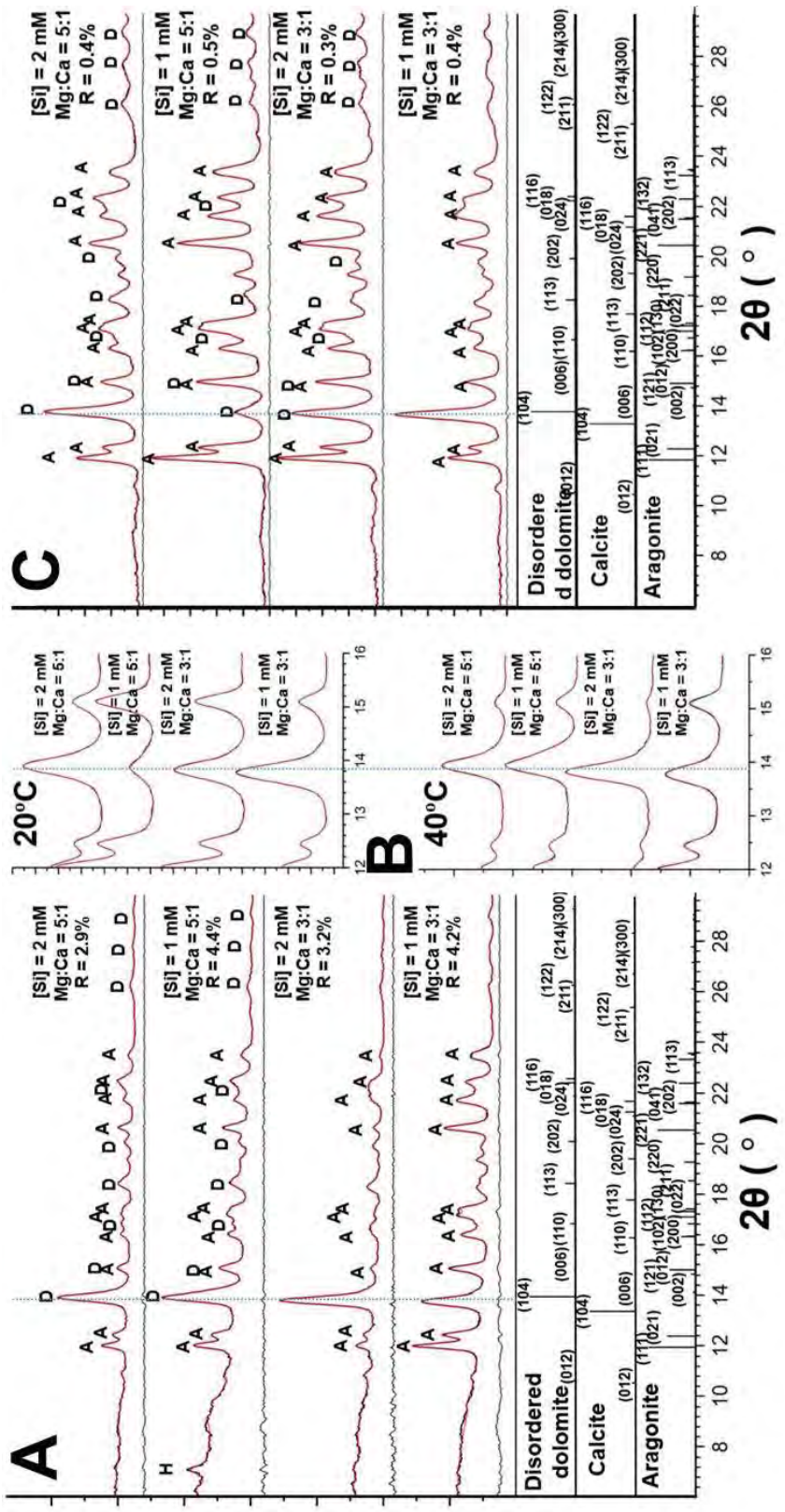

Figure 1

This is the peer-reviewed, final accepted version for American Mineralogist, published by the Mineralogical Society of America.
The published version is subject to change. Cite as Authors (Year) Title. American Mineralogist, in press.
DOI: https://doi.org/10.2138/am-2021-7474. http://www.minsocam.org/

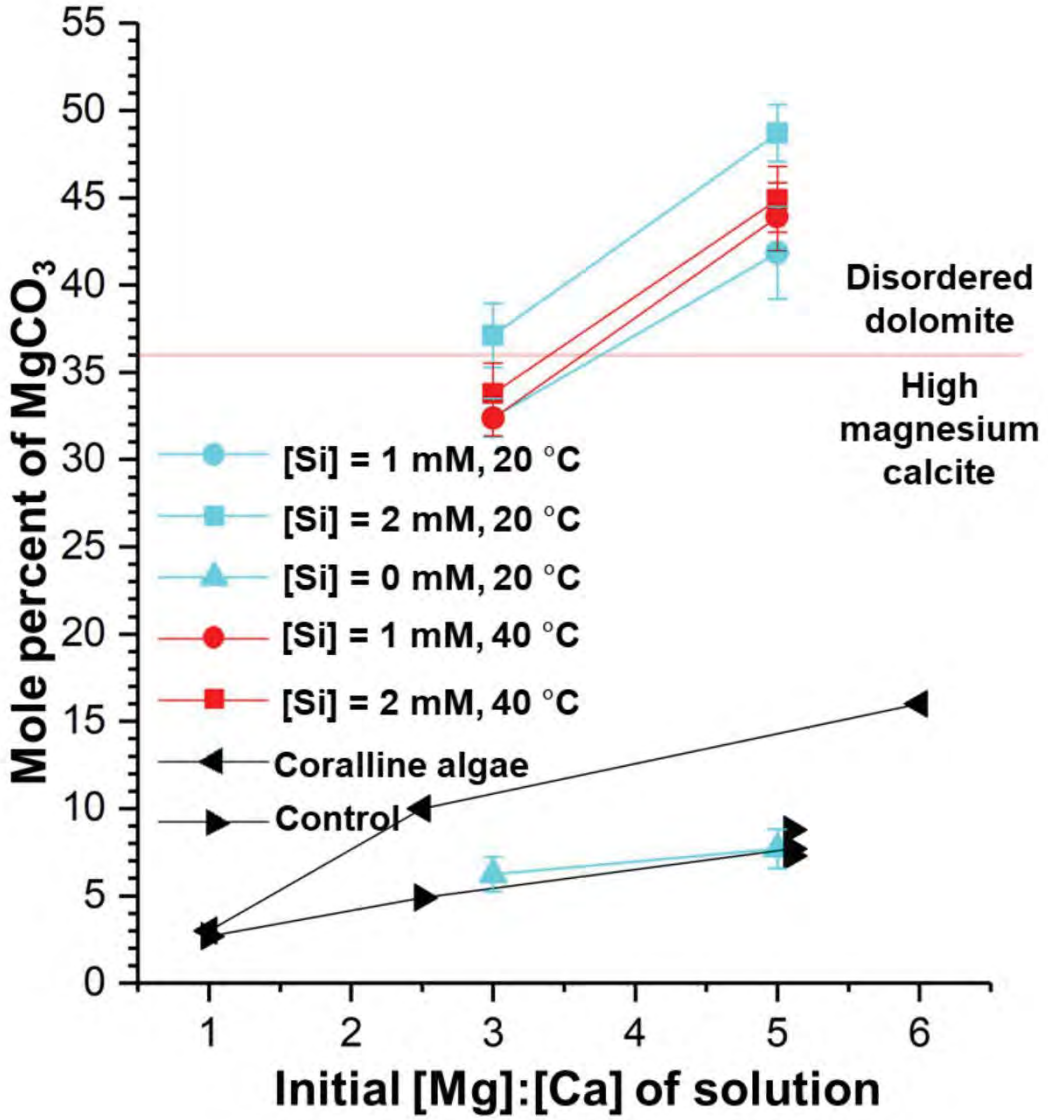

Figure 2

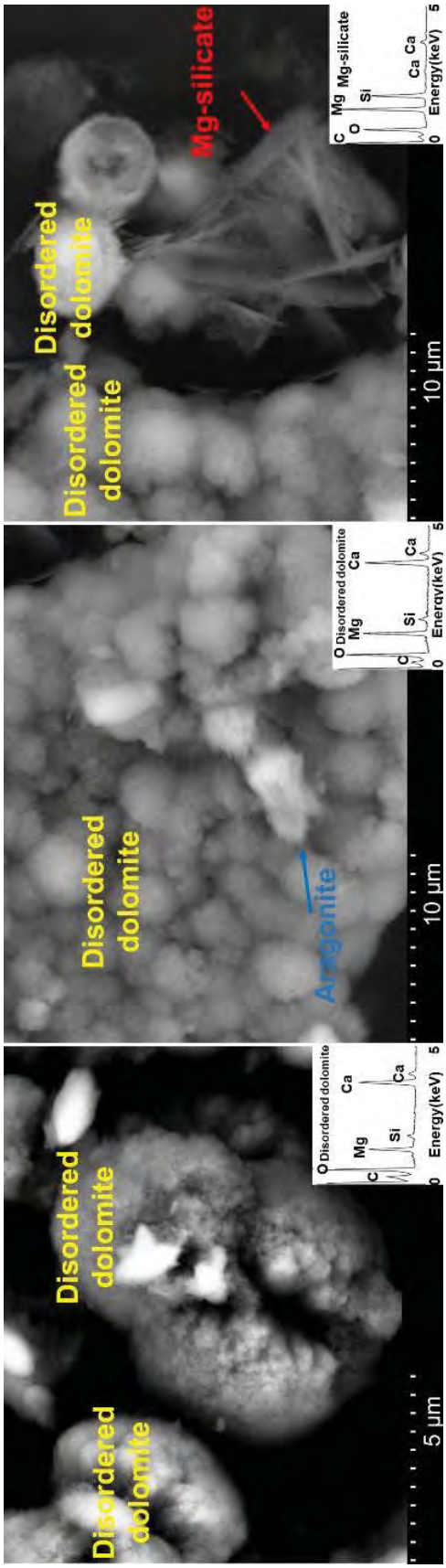

Figure 3

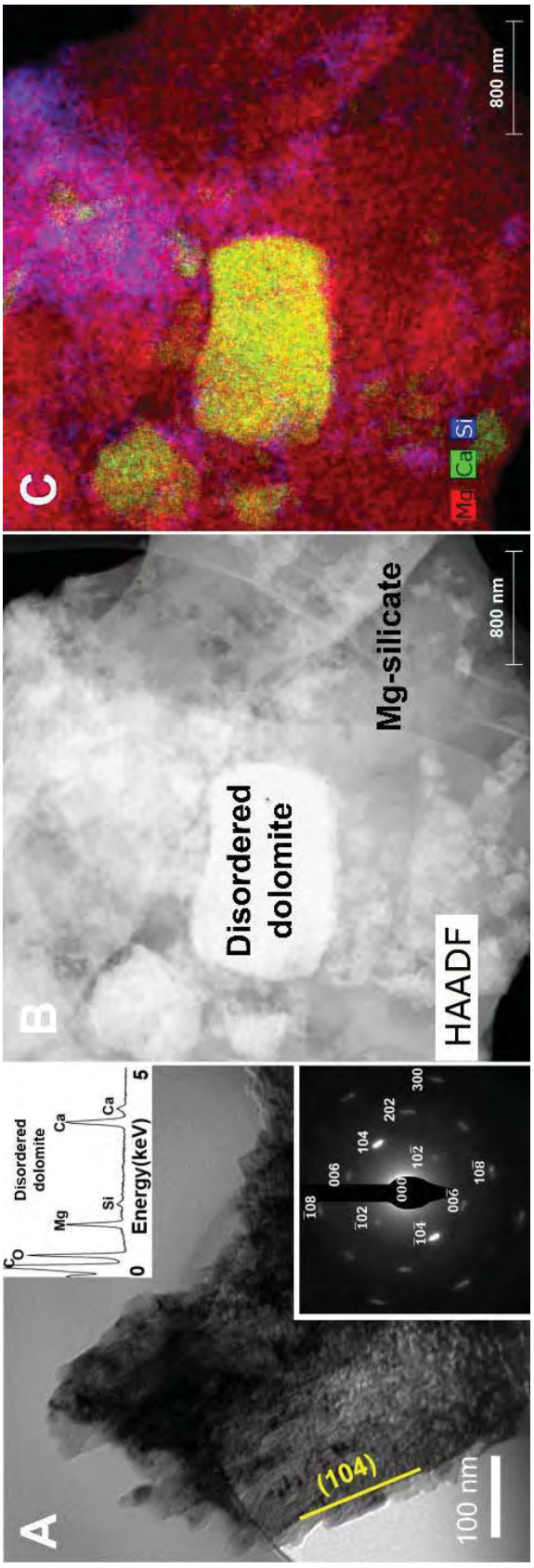

Figure 4

This is the peer-reviewed, final accepted version for American Mineralogist, published by the Mineralogical Society of America.
The published version is subject to change. Cite as Authors (Year) Title. American Mineralogist, in press.
DOI: https://doi.org/10.2138/am-2021-7474. http://www.minsocam.org/

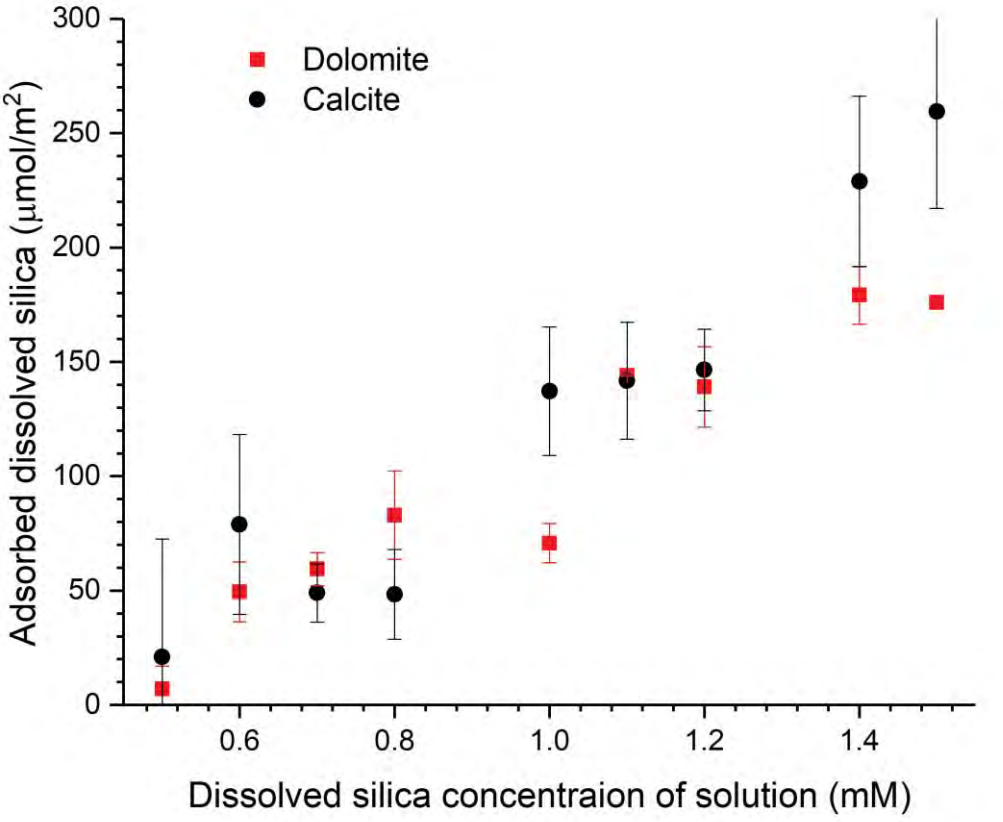

Figure 5

This is the peer-reviewed, final accepted version for American Mineralogist, published by the Mineralogical Society of America.
The published version is subject to change. Cite as Authors (Year) Title. American Mineralogist, in press.
DOI: https://doi.org/10.2138/am-2021-7474. http://www.minsocam.org/

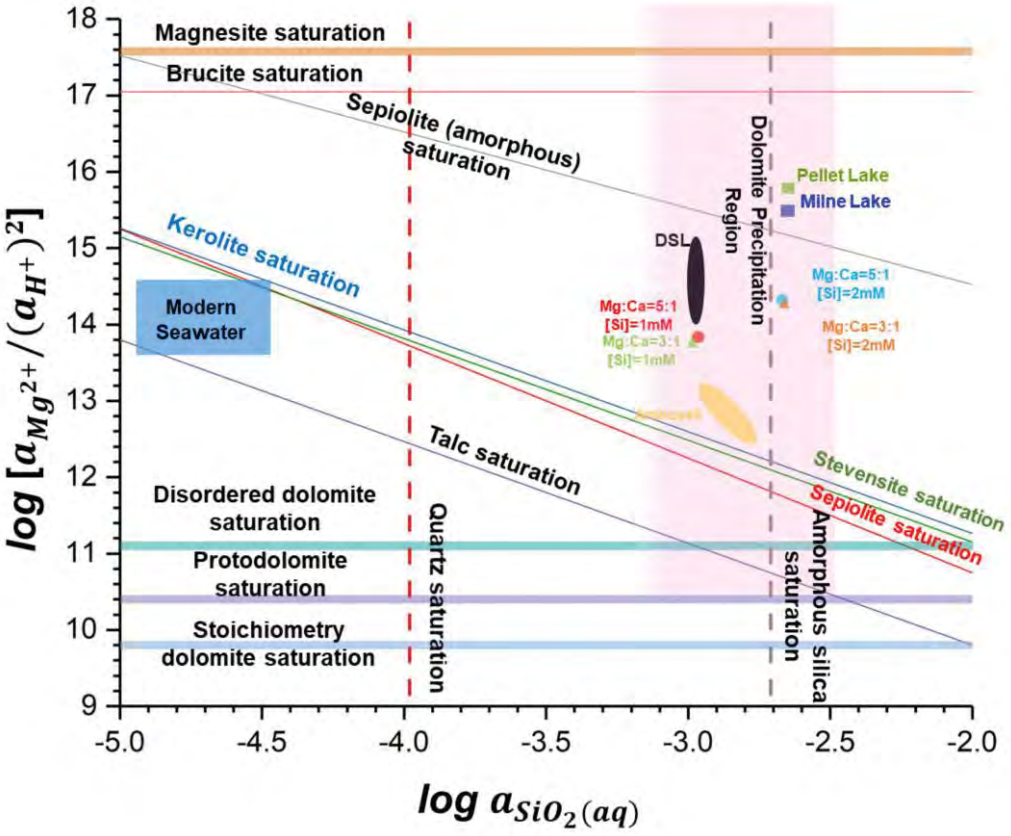

Figure 6

This is the peer-reviewed, final accepted version for American Mineralogist, published by the Mineralogical Society of America.
The published version is subject to change. Cite as Authors (Year) Title. American Mineralogist, in press.
DOI: https://doi.org/10.2138/am-2021-7474. http://www.minsocam.org/

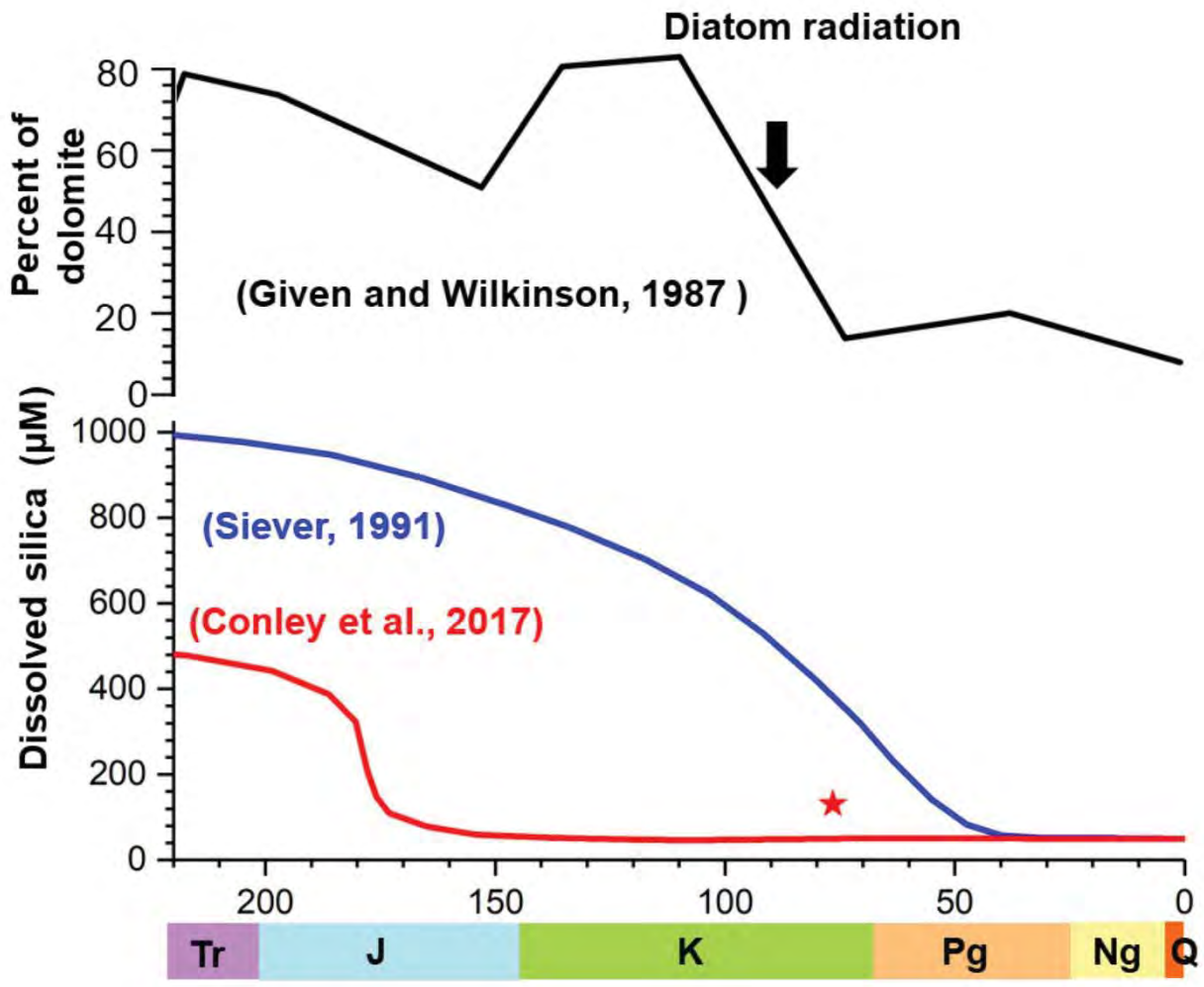

Figure 7